






# Small-Signal Stability Analysis of a VSC-MTDC System for Investigating DC Voltage Oscillation

Qiang Fu , Wenjuan Du , Member, IEEE, Haifeng Wang , Senior Member, IEEE, Bixing Ren ,  
and Xianyong Xiao 

**Abstract**—In this study, the DC voltage oscillation mechanism is investigated based on the linearized models of a voltage-source converter (VSC)-based multiple terminal DC (MTDC) system. First, the mechanism of DC voltage oscillation generation is revealed. DC voltage or DC voltage droop-controlled VSCs are identified as the DC voltage oscillation sources when master-slave or DC voltage droop control is separately applied to the VSC-MTDC system. Meanwhile, the active power-controlled VSC is equally regarded as a constant power source that does not provide any oscillation to the VSC-MTDC system. Subsequently, the impact of the dynamics of VSCs and MTDC network on the DC voltage oscillation is separately investigated. It is theoretically verified that the negative eigenvalues of the MTDC network conductance matrix can reduce the stability of the DC voltage oscillation. The constant power load is identified as the physical mechanism of a problematic scenario that induces DC voltage oscillation in the generalized VSC-MTDC system. Moreover, it is demonstrated for the first time that the steady-state power flow may cause DC voltage oscillations when the power flow is reversed. Finally, two VSC-MTDC systems, which individually adopt master-slave and DC voltage droop control, are presented to validate the findings using the standard MATLAB SIMULINK model.

**Index Terms**—DC voltage oscillation, MTDC power system, Power flow, Small-signal stability.

## NOMENCLATURE

$C_k$ :	Capacitance on the DC side of the $k^{\text{th}}$ VSC
$\bar{V}_k$ :	DC voltage of the $k^{\text{th}}$ VSC
$\bar{I}_{netk}$ :	DC current at the input of $C_k$ from the DC network
$\bar{I}_k$ :	DC current at the output of $C_k$
$X_k$ :	Reactance of the filter on the AC side of the $k^{\text{th}}$ VSC
$\bar{I}_{dk}$ :	AC current in $d$ axis

Manuscript received June 28, 2020; revised October 20, 2020, December 22, 2020, and February 23, 2021; accepted March 27, 2021. Date of publication April 12, 2021; date of current version October 20, 2021. This work supported in part by the Engineering Special Team of Sichuan University on New Energy Power Systems and in part by the National Key Research and Development Program of China under Grant 2016YFB0900602 and in part by the Fundamental Research Funds for the Central Universities under Grant YJ201654. (Corresponding author: Wenjuan Du.)

Qiang Fu, Wenjuan Du, Haifeng Wang, and Xianyong Xiao are with the School of Electrical Engineering, Sichuan University, Chengdu 610065, China (e-mail: 1197348393@qq.com; ddwenjuan@gmail.com; hfwang60@qq.com; xiaoxianyong@163.com).

Bixing Ren is with the State Grid Jiangsu Electric Power Co. Ltd. Research Institute, Nanjing 211103, China (e-mail: renbixing@126.com).

Color versions of one or more figures in this article are available at <https://doi.org/10.1109/TPWRS.2021.3072399>.

Digital Object Identifier 10.1109/TPWRS.2021.3072399

$\tilde{I}_{qk}$ :	AC current in $q$ axis
$P_k$ :	Active power at the output of the $k^{\text{th}}$ VSC
$\tilde{V}_k$ :	AC voltage at the point of common coupling
$\tilde{V}_{dk}$ :	$d$ -axis component of $\tilde{V}_k$
$\tilde{V}_{qk}$ :	$q$ -axis component of $\tilde{V}_k$
$\tilde{V}_{ck}$ :	AC voltage at the terminal of the AC-DC converter
$\tilde{V}_{cdk}$ :	$d$ -axis component of $\tilde{V}_{ck}$
$\tilde{V}_{cqk}$ :	$q$ -axis component of $\tilde{V}_{ck}$
$\omega_0$ :	Synchronous frequency
$\omega_m$ :	Frequency of the DC voltage oscillation mode of the master-slave-controlled VSC-MTDC power system
$\omega_{dw}$ :	Frequency of the worst DC voltage oscillation mode of the DC voltage-controlled VSC-MTDC power system
$K_{pk} + K_{ik}s^{-1}$ :	Transfer function of the outer control loop of the $k^{\text{th}}$ VSC
$K_{pk}^c + K_{ik}^cs^{-1}$ :	Transfer function of the inner control loop of the $k^{\text{th}}$ VSC
$\mathbf{x}_1^m$ :	Vector of all state variables of the DC voltage-controlled VSC
$\mathbf{a}_1^m, \mathbf{b}_1^m$ , and $\mathbf{c}_1^m$ :	State matrix, control vector, and output vector of the state-space model of the DC voltage-controlled VSC, respectively
$\mathbf{x}_j^m$ :	Vector of all state variables of the active power-controlled VSC
$\mathbf{a}_j^m, \mathbf{b}_j^m$ , and $\mathbf{c}_j^m$ :	State matrix, control vector, and output vector of the state-space model of the active power-controlled VSC, respectively
$\mathbf{x}_f^d$ :	Vector of all state variables of the DC voltage droop-controlled VSC
$\mathbf{a}_f^d, \mathbf{b}_f^d$ , and $\mathbf{c}_f^d$ :	State matrix, control vector, and output vector of the state-space model of the DC voltage droop-controlled VSC, respectively
$\mathbf{X}_d$ :	Vector of all state variables of M-N DC voltage droop-controlled VSCs
$\mathbf{A}_d, \mathbf{B}_d$ , and $\mathbf{C}_d$ :	State matrix, control vector, and output vector of the state-space model of M-N DC voltage droop-controlled VSCs, respectively
$\Delta$ :	Small increment in a variable
$\mathbf{E}$ :	Identity matrix
$\mathbf{0}$ :	Zero matrix
$\text{diag}$ :	Diagonal block matrix

Subscript $k$ :	Number identifier of all VSCs
Subscript $j$ :	Number identifier of the active power-controlled VSCs
Subscript $f$ :	Number identifier of the DC voltage droop-controlled VSCs
Superscript $ref$ :	Reference value of the control system

## I. INTRODUCTION

VOLTAGE-SOURCE converters (VSCs) have been widely used for power generation and DC transmission owing to their technical advantages. A VSC-based multiple terminal DC (VSC-MTDC) power system can connect multiple AC power systems and enhance the flexibility of AC/DC hybrid power systems [1]–[2].

The stability of DC voltage oscillation has been a major issue that has been actively investigated in recent years. Two main problems concerning the small-signal DC voltage stability of VSC-MTDC power systems have been identified. The first is the instability caused by the dynamic interaction between AC and DC power systems. Studies addressing this problem assumed that the independent AC and DC power systems were respectively stable. However, integrating AC and DC power systems can induce instability problems [3]–[6] because the dynamic interaction between the AC and DC power systems has a negative impact on the stability of an AC/DC hybrid power system. The second is the instability caused by the dynamic interactions between the VSCs and DC network [7]–[10] in a standalone DC power system. The stability of DC voltage oscillation as one of the stability issues in a standalone DC power system has attracted the attention of many researchers. To evaluate how DC impact factors affect the stability of a DC power system, the dynamics of the AC power system were ignored and the AC power system was represented using an infinite bus. This study focuses on the second problem.

Thus far, the stability of small-signal DC voltage oscillation has been numerically analyzed using modal analysis [11]–[13] and frequency domain analysis [14]–[16]. In the modal analysis of DC voltage oscillation, the DC voltage oscillation modes were analyzed using the state-space model. The DC voltage oscillation was damped if the DC oscillation mode was located on the left side of the complex plane. Moreover, this investigation can be conducted by focusing on certain aspects of the MTDC power system stability using participation factors. In [11], a detailed modal analysis assisted by computational results of participation factors was presented. Results indicated that the damping ratio of the DC voltage oscillation could be improved by accurately tuning the control loop parameters. In [12], a scheme was proposed for adapting the droop coefficients to share the power load according to the available headroom of each converter station. The influence of varying the droop coefficients on the stability of the MTDC power system was analyzed using modal analysis [12]. The study presented in [13] well demonstrated the effectiveness of modal analysis, which can assist in identifying possible sources of negative interactions between VSCs.

Impedance-model-based analysis (IMA) is representative of frequency domain analysis. A series of investigations on the DC voltage oscillation of the MTDC power system were conducted in [14]–[16]; results indicated that instability was caused by the negative resistance from the VSC control systems. In [14], IMA was used to investigate the DC voltage instability from the perspective of negative resistance. In [15], it was reported that the frequency of DC voltage oscillation is approximately 10 Hz and the fast dynamics of the VSC's control loops can be ignored for simplification. In this case, the modal resonance between the oscillation modes of the phase-locked loop (PLL) and DC voltage control in a VSC can cause DC voltage instability.

However, both modal analysis and IMA of power systems rely on numerical results. DC voltage oscillation instability occurs when the real part of the DC voltage oscillation mode is positive or the impedance of the DC equipment is negative [11]–[16]. An in-depth evaluation for identifying the reasons for the real part of the DC voltage oscillation mode being positive or the impedance of the DC equipment being negative has not been conducted. Hence, identifying risky conditions and further investigating the physical causes that result in the DC voltage oscillation instability are essential. Moreover, an HVDC line is generally considered for analyzing a simple DC power system because it is a low-order system and can be easily transformed into a single-input single-output system for IMA. In the VSC-MTDC power system, employing modal analysis is time consuming and IMA is challenging because it is a multiple-input multiple-output system. Further, the dynamics of VSCs are generally considered the main cause of the DC voltage oscillation instability, while the impact of steady-state power flow has received less attention.

In this paper, DC voltage oscillations are theoretically studied and verified using the standard MATLAB SIMULINK model. The mechanism of the generation of DC voltage oscillation is elucidated. Moreover, the effects of the dynamics of VSCs and MTDC network on DC voltage oscillation are explained. Inspired by [14] and [17], we demonstrate for the first time that steady-state power flow can negatively affect DC voltage oscillation when the power flow is reversed. This finding confirms that the dynamics of the MTDC power system as well as the steady-state power flow affect the stability of the DC voltage oscillation. The contributions of this paper are as follows:

- 1) The generation of DC voltage oscillation is explained. It is demonstrated that a VSC that adopts DC voltage control or DC voltage droop control is the source of DC voltage oscillation.
- 2) The individual impacts of the dynamics of VSCs and MTDC network on DC voltage oscillation are clarified. DC voltage oscillation can become unstable if the open-loop VSC parameters are not appropriately designed or the eigenvalue of the MTDC network conductance matrix is negative.
- 3) It is theoretically confirmed that steady-state power flow can also decrease the stability of DC voltage oscillation when the power flow is reversed. This result is further verified using the standard model in MATLAB SIMULINK.

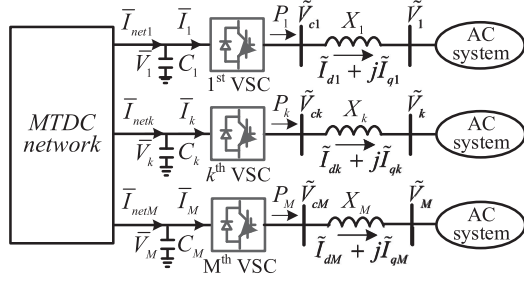
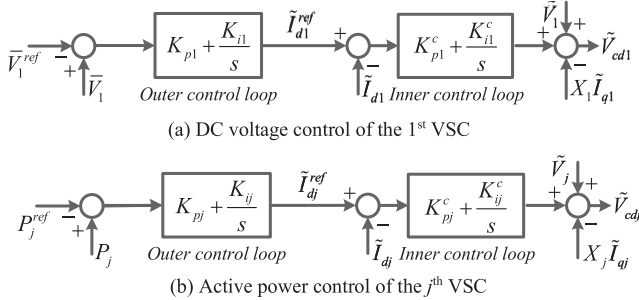


Fig. 1. Configuration of the VSC-MTDC power system.


 Fig. 2. Configuration of the  $M$  VSC control systems (a) DC voltage control of the 1<sup>st</sup> VSC (b) Active power control of the  $j^{\text{th}}$  VSC.

## II. MASTER-SLAVE-CONTROLLED VSC-MTDC POWER SYSTEM

The configuration of a VSC-MTDC power system connected with  $M$  VSCs is shown in Fig. 1. Considering that this study mainly focuses on the stability of DC voltage oscillation in the MTDC power system, VSCs are separately connected to  $M$  AC systems represented by infinite buses [7]–[8], [10]. Thus, the dynamics of the AC systems are ignored with  $\Delta \tilde{V}_k = 0$  and  $k = 1, 2, \dots, M$ . Assuming that the direction of  $\tilde{V}_k$  is along the  $d$  axis of the VSC  $d$ - $q$  coordinate system (i.e.,  $\tilde{V}_{qk} = 0$ ,  $\tilde{V}_{dk} = \tilde{V}_k$ ), we obtain

$$P_k = \tilde{V}_k \tilde{I}_{dk} = \tilde{V}_k \tilde{I}_k \quad (1)$$

It is assumed that the 1<sup>st</sup> VSC uses DC voltage control and the rest of the VSCs (i.e.,  $j^{\text{th}}$  VSC,  $j = 2, 3, \dots, M$ ) use active power control. These configurations are shown in Fig. 2 [11].

Regarding the  $k^{\text{th}}$  VSC, the dynamic equation of the DC voltage is obtained as

$$C_k \frac{d\tilde{V}_k}{dt} = \tilde{I}_{netk} - \frac{P_k}{\tilde{V}_k} \quad (2)$$

The dynamic equation of the AC current in  $d$  axis is

$$X_k \omega_0^{-1} \frac{d\tilde{I}_{dk}}{dt} = X_k \tilde{I}_{qk} + \tilde{V}_{cdk} - \tilde{V}_k \quad (3)$$

The dynamic equation of the inner control loop is obtained from Fig. 2 to be

$$\tilde{V}_{cdk} = \tilde{V}_k - X_k \tilde{I}_{qk} + \left( K_{pk}^c + \frac{K_{ik}^c}{s} \right) (\tilde{I}_{dk}^{ref} - \tilde{I}_{dk}) \quad (4)$$

Substituting (4) into (3), yields

$$\tilde{I}_{dk} = G_{idk}(s) \tilde{I}_{dk}^{ref} \quad (5)$$

where,

$$G_{idk}(s) = \frac{K_{pk}^c s + K_{ik}^c}{X_k \omega_0^{-1} s^2 + K_{pk}^c s + K_{ik}^c}$$

In (5),  $G_{idk}(s)$  represents the dynamics of the inner current loop. It is indicated in [15]–[16] that considering the different response speeds of the inner current (around 10 ms) and outer DC voltage control loops (around 100 ms), dynamics in these two timescales can be analyzed individually, due to their relatively separated response times. Therefore, for dynamic analysis in DC voltage oscillation timescale, AC currents can be considered to instantaneously track their reference values. Thus,  $G_{idk}(s)$  is approximately equal to 1 and (5) can be simplified to be  $\tilde{I}_{dk} = \tilde{I}_{dk}^{ref}$ .

### A. Linearized Model of the DC Voltage-Controlled VSC

Based on Fig. 2(a), the transfer function of the outer control loop of the 1<sup>st</sup> VSC is obtained as

$$\tilde{I}_{d1}^{ref} = \left( K_{p1}^c + \frac{K_{i1}^c}{s} \right) (\tilde{V}_1 - \tilde{V}_1^{ref}) \quad (6)$$

By linearizing (1), (2), and (6) at a steady state, the linearized model of the 1<sup>st</sup> VSC to analyze the DC voltage oscillation is obtained as follows (refer to (A1) in Appendix A for details):

$$s \mathbf{x}_1^m = \mathbf{a}_1^m \mathbf{x}_1^m + \mathbf{b}_1^m \Delta \tilde{I}_{net1}, \Delta \tilde{V}_1 = \mathbf{c}_1^m \mathbf{x}_1^m \quad (7)$$

Furthermore, the dynamics of the 1<sup>st</sup> VSC can be represented using the following transfer function:

$$\begin{aligned} \Delta \tilde{V}_1 &= \mathbf{c}_1^m (s \mathbf{E} - \mathbf{a}_1^m)^{-1} \mathbf{b}_1^m \Delta \tilde{I}_{net1} \\ &= \frac{s \tilde{V}_1}{K_1^m s^2 + K_2^m s + K_3^m} \Delta \tilde{I}_{net1} \end{aligned} \quad (8)$$

where  $K_1^m = C_1 \tilde{V}_1$ ,  $K_2^m = (K_{p1} \tilde{V}_1 - \tilde{I}_1)$ , and  $K_3^m = K_{i1} \tilde{V}_1$ .

According to (1), the variation in the active power output from the 1<sup>st</sup> VSC can be obtained as

$$\Delta P_1 = \frac{\tilde{V}_1 \tilde{V}_1 (K_{p1} s + K_{i1})}{K_1^m s^2 + K_2^m s + K_3^m} \Delta \tilde{I}_{net1} \quad (9)$$

### B. Linearized Model of the Active Power-Controlled VSC

Based on Fig. 2(b), the transfer function of the outer control loop of the  $j^{\text{th}}$  VSC is obtained as

$$\tilde{I}_{dj}^{ref} = \left( K_{pj} + \frac{K_{ij}}{s} \right) (P_j - P_j^{ref}) \quad (10)$$

By linearizing (1), (2), and (10) at a steady state, the linearized model of the  $j^{\text{th}}$  VSC is obtained as follows (refer to (A2) in Appendix A for details):

$$s \mathbf{x}_j^m = \mathbf{a}_j^m \mathbf{x}_j^m + \mathbf{b}_j^m \Delta \tilde{I}_{netj}, \Delta \tilde{V}_j = \mathbf{c}_j^m \mathbf{x}_j^m \quad (11)$$

The transfer function of  $\Delta \tilde{V}_j$  is represented by

$$\Delta \tilde{V}_j = \frac{-\tilde{V}_j}{\tilde{I}_j - s C_j \tilde{V}_j} \Delta \tilde{I}_{netj} = R_{ej}(s) \Delta \tilde{I}_{netj} \quad (12)$$

The variation in the active power output from the  $j^{\text{th}}$  VSC is obtained as

$$\Delta P_j = 0 \quad (13)$$

From (9) and (13), the active power response of VSCs differs when a different control is adopted, resulting in different effects on the dynamics of the VSC-MTDC power system. The active power response of the DC voltage-controlled VSC is oscillatory, which can induce oscillations in the VSC-MTDC power system. However, the active power response of the active power-controlled VSC is stationary, which is similar to that of a constant power source, and it does not provide any oscillation to the VSC-MTDC power system. Therefore, when master-slave control is applied to the VSC-MTDC power system, the DC voltage oscillation is predominantly induced by the DC voltage-controlled VSC rather than the active power-controlled VSC. This oscillation is propagated to other VSCs through the MTDC network. Considering that there is no active power response of the active power-controlled VSCs, the DC capacitors of  $M - 1$  active power-controlled VSCs respond to the oscillating active power to maintain power balance.

### C. Linearized Model of the VSC-MTDC Power System

The transfer function of the MTDC network is

$$\begin{bmatrix} \Delta \bar{I}_{net1} \\ \Delta \bar{I}_{netr} \end{bmatrix} = - \begin{bmatrix} y_{11} & \mathbf{y}_{1M} \\ \mathbf{y}_{M1} & \mathbf{y}_{MM} \end{bmatrix} \begin{bmatrix} \Delta \bar{V}_1 \\ \Delta \bar{\mathbf{V}}_r \end{bmatrix} \quad (14)$$

where  $\Delta \bar{\mathbf{I}}_{netr} = [\Delta \bar{I}_{net2} \dots \Delta \bar{I}_{netM}]^T$  and  $\Delta \bar{\mathbf{V}}_r = [\Delta \bar{V}_2 \dots \Delta \bar{V}_M]^T$ .  $y_{11}$ ,  $\mathbf{y}_{1M}$ ,  $\mathbf{y}_{M1}$ , and  $\mathbf{y}_{MM}$  are the elements of the MTDC network conductance matrix.

Substituting (12) into (14) yields

$$\Delta \bar{I}_{net1} = -Y_m(s) \Delta \bar{V}_1 \quad (15)$$

where  $Y_m(s) = y_{11} - \mathbf{y}_{1M} \mathbf{R}(s) [\mathbf{E} + \mathbf{R}(s) \mathbf{y}_{MM}]^{-1} \mathbf{y}_{M1}$  and  $\mathbf{R}(s) = \text{diag}(R_{ej}(s))$ .

By substituting (15) into (8), the characteristic equation of the VSC-MTDC power system can be obtained as

$$\mathbf{c}_1^m (s\mathbf{E} - \mathbf{a}_1^m)^{-1} \mathbf{b}_1^m + Y_m(s)^{-1} = 0 \quad (16)$$

In (16), the two-order part of  $\mathbf{c}_1^m (s\mathbf{E} - \mathbf{a}_1^m)^{-1} \mathbf{b}_1^m$  is generated by the DC voltage-controlled VSC. Moreover, the dynamics of  $Y_m(s)^{-1}$  are formed by the DC network and capacitors of  $M - 1$  active power-controlled VSCs. These two parts are coupled via the DC network, and they collectively determine the stability of DC voltage oscillation. Therefore, the DC voltage-controlled VSC itself and the DC network, including the active power-controlled VSCs, are the two main factors that impact the stability of DC voltage oscillation.

### D. Stability Analysis of DC Voltage Oscillation

$\lambda_{m0} = -\varepsilon_{m0} + j\omega_{m0}$  represents the open-loop DC voltage oscillation mode of the 1<sup>st</sup> VSC, i.e., the solution of  $|s\mathbf{I} - \mathbf{a}_1^m| = 0$ .

The damping ratio of  $\lambda_{m0}$  is  $d_{m0} = \varepsilon_{m0}(\sqrt{\varepsilon_{m0}^2 + \omega_{m0}^2})^{-1}$ . The 1<sup>st</sup> VSC is self-stable, and its impact is positive if  $\varepsilon_{m0} > 0$ ,

which yields

$$\bar{I}_1 - \bar{V}_1 K_{p1} < 0 \quad (17)$$

$\lambda_m = -\varepsilon_m + j\omega_m$  denotes the closed-loop DC voltage oscillation mode corresponding to  $\lambda_{m0}$  of the MTDC power system, i.e., the solution of (16). The damping ratio of  $\lambda_m$  is

$d_m = \varepsilon_m(\sqrt{\varepsilon_m^2 + \omega_m^2})^{-1}$ . Thus, the impact of the MTDC network on the DC voltage oscillation can be evaluated using  $\Delta d_m$ , where  $\Delta d_m = d_m - d_{m0}$ , which is positive if  $\Delta d_m > 0$ .

At frequency  $\omega_m$ ,  $Y_m(j\omega_m) = G_m(\omega_m) + jH_m(\omega_m)$ . Thus, (16) can be simplified for approximately calculating  $\Delta d_m$  using the equation below [18]–[19]

$$\begin{aligned} \mathbf{c}_1^m (s\mathbf{E} - \mathbf{a}_1^m)^{-1} \mathbf{b}_1^m + Y_m(j\omega_m)^{-1} &= 0 \\ &= \frac{s\bar{V}_1}{K_1^m s^2 + K_2^m s + K_3^m} + \frac{1}{G_m(\omega_m) + jH_m(\omega_m)} \\ &\approx K_1^m s^2 + K_2^m s + K_3^m + s\bar{V}_1 G_m(\omega_m) \\ &\quad - \omega_m \bar{V}_1 H_m(\omega_m) = 0 \end{aligned} \quad (18)$$

From (18),  $\Delta d_m$  can be calculated as

$$\Delta d_m = \frac{1}{2} \left( \frac{K_2^m + \bar{V}_1 G_m(\omega_m)}{\sqrt{K_1^m (K_3^m - \omega_m \bar{V}_1 H_m(\omega_m))}} - \frac{K_2^m}{\sqrt{K_1^m K_3^m}} \right) \quad (19)$$

Considering that the values of  $\bar{V}_1$ ,  $K_1^m$  and  $K_2^m$  are positive, (19) indicates that  $\Delta d_m$  increases if  $G_m(\omega_m)$  increases. The damping ratio of  $\lambda_m$  is better than that of  $\lambda_{m0}$  and thus, the DC voltage oscillation is well damped if

$$G_m(\omega_m) > \frac{K_2^m}{\bar{V}_1} \left( \sqrt{1 - \frac{\omega_m \bar{V}_1 H_m(\omega_m)}{K_3^m}} - 1 \right) \quad (20)$$

It can be seen from (20) that the criterion changes with the change in  $\omega_m$  and  $H_m(\omega_m)$ . A positive  $G_m(\omega_m)$  is more likely to satisfy the condition and improve the DC voltage stability than a negative  $G_m(\omega_m)$ . If (20) is not satisfied, then  $\Delta d_m < 0$  and the damping ratio of  $\lambda_m$  decreases. In this case, the MTDC power system can suffer from DC voltage oscillation instability. This result indicates that the MTDC power system can be unstable even if VSCs are self-stable. Therefore, the MTDC network must receive significant attention. Herein,  $G_m(\omega_m)$  obviously plays an important role because it can reveal the physical condition that induces  $\Delta d_m$  to become negative. This approach is useful as it clarifies the mechanism of DC voltage oscillation instability.

$G_m(\omega_m)$  is closely related to the power flow because the parameters of the transmission line are constant. Hereby, a two-terminal VSC-based power system ( $M = 2$  in Fig. 1) is an explanatory example, where the 1<sup>st</sup> and 2<sup>nd</sup> VSCs adopt DC voltage control and active power control, respectively. At frequency  $\omega_m$ , we obtain

$$G_m(\omega_m) = y_{11} - \frac{y_{12}y_{21}(\bar{I}_{net2}\bar{V}_2^{-1} + y_{22})}{(\bar{I}_{net2}\bar{V}_2^{-1} + y_{22})^2 + (\omega_m C_2)^2} \quad (21)$$

where  $y_{11}$ ,  $y_{12}$ ,  $y_{21}$ , and  $y_{22}$  are the positive elements of the DC conductance matrix.



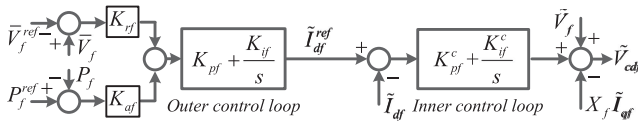


Fig. 3. Configuration of the DC voltage droop control.

From (21),  $G_m(\omega_m)$  is shown to be closely related to the power flow of the 2<sup>nd</sup> VSC.  $G_m(\omega_m)$  decreases when the 2<sup>nd</sup> VSC changes its function from power dispersion ( $\bar{I}_{net2} < 0$ ) to power absorption ( $\bar{I}_{net2} > 0$ ). A decrease in  $G_m(\omega_m)$  may result in  $\Delta d_m < 0$ , which further demonstrates that the power flow can affect the stability of DC voltage oscillation. When the power flow is reversed, constant power loads are achieved and  $G_m(\omega_m)$  is decreased, which increases the risk of breaking the condition listed in (20). Hence, constant power loads are dangerous for the MTDC power system. For safety purposes, the capacity of the constant power loads should be restricted. The limitation of  $G_m(\omega_m)$  can be obtained as  $G_{lim}$  by solving the following equation:

$$d_m = \frac{K_2^m + \bar{V}_1 G_m(\omega_m)}{2\sqrt{K_1^m(K_3^m - \omega_m \bar{V}_1 H_m(\omega_m))}} = 0 \quad (22)$$

Generally, the parameters of VSCs are appropriately designed such that  $\lambda_{m0}$  is well damped. Therefore, the instability of the DC voltage oscillation is mainly caused by constant power loads, which can occur when the power flow is reversed. In this case, the system does not immediately lose its stability because of the stability margin of the VSC itself.

The DC voltage oscillation can occur if the following limitation is exceeded:

$$G_m(\omega_m) > G_{lim}. \quad (23)$$

It is indicated that  $\omega_m$  should be calculated by (16) or measured by a specific case. However, during the stability evaluation, there are many scenarios needed to be evaluated. It is time consuming if we calculate  $\omega_m$  for each scenario. Therefore, the range of  $\omega_m$  is determined to be  $\omega_{max} \geq \omega_m \geq \omega_{min}$  so that the frequency range could cover all possible  $\omega_m$  under any condition. Based on which, the instability risk can be detected by sweeping the frequency in the range rather calculating  $\omega_m$  for each scenario, which is useful to quickly determine the stability risk of the DC voltage oscillation. The range of  $\omega_m$  can be decided by referring the open-loop oscillation frequency  $\omega_{m0}$ , such as that  $\omega_{max} = k_1 \omega_{m0}$ ,  $\omega_{min} = k_2 \omega_{m0}$ , where  $k_1$  and  $k_2$  are coefficients and satisfy  $k_1 > 1$  and  $0 < k_2 < 1$ . In the frequency range, the minimum value of  $G_m(j\omega_m)$ ,  $\omega_m \in [\omega_{min}, \omega_{max}]$ , is denoted as  $G_{min}$  and the stability of the DC voltage oscillation can be quickly evaluated by comparing  $G_{min}$  and  $G_{lim}$ .

### III. DC VOLTAGE DROOP-CONTROLLED VSC-MTDC POWER SYSTEM

#### A. Linearized Model of the DC Voltage Droop-Controlled VSC

The configuration of the DC voltage droop control is shown in Fig. 3. In this case,  $M - N$  VSCs adopt DC voltage droop

control, whereas the remaining  $N$  VSCs adopt active power control. Based on Fig. 3, the transfer function of the outer control loop of the  $f^{\text{th}}$  VSC ( $f = 1, 2, \dots, M - N$ ) is obtained as

$$\tilde{I}_{df}^{ref} = \left( K_{pf} + \frac{K_{if}}{s} \right) \left( K_{rf} \left( \bar{V}_f - \bar{V}_f^{ref} \right) + K_{af} \left( P_f^{ref} - P_f \right) \right) \quad (24)$$

By linearizing (1), (2), and (24) at a steady state, the linearized model of the  $f^{\text{th}}$  VSC is obtained as follows (refer to (A3) in Appendix A for details):

$$s\mathbf{x}_f^d = \mathbf{a}_f^d \mathbf{x}_f^d + \mathbf{b}_f^d \Delta \bar{I}_{netf}, \Delta \bar{V}_f = \mathbf{c}_f^d \mathbf{x}_f^d \quad (25)$$

The transfer function of  $\Delta \bar{V}_f$  is

$$\begin{aligned} \Delta \bar{V}_f &= \mathbf{c}_f^d (s\mathbf{E} - \mathbf{a}_f^d)^{-1} \mathbf{b}_f^d \Delta \bar{I}_{netf} \\ &= \frac{H_f^d(s)}{K_{f-1}^d s^2 + K_{f-2}^d s + K_{f-3}^d} \Delta \bar{I}_{netf} \end{aligned} \quad (26)$$

where

$$\begin{aligned} K_{f-1}^d &= C_f \bar{V}_f + C_f \bar{V}_f \tilde{V}_f K_{pf} K_{af} \\ K_{f-2}^d &= \bar{I}_f + C_f \bar{V}_f \tilde{V}_f K_{if} K_{af} \\ &\quad + \bar{I}_f \tilde{V}_f K_{pf} K_{af} - \tilde{V}_f K_{pf} K_{rf} \\ K_{f-3}^d &= \bar{I}_f \tilde{V}_f K_{if} K_{af} - \tilde{V}_f K_{if} K_{rf} \\ H_f^d(s) &= (\bar{V}_f + \bar{V}_f \tilde{V}_f K_{af} K_{pf})s + \bar{V}_f \tilde{V}_f K_{af} K_{if} \end{aligned}$$

A comparison between (26) and (8) shows that both the DC voltage-controlled VSC and DC voltage droop-controlled VSC exhibit a two-order loop. Hence, when DC voltage droop control is applied to the VSC-MTDC power system, the DC voltage oscillation is mainly induced by the DC voltage droop-controlled VSCs rather than the active power-controlled VSCs. The transfer function of  $M - N$  VSCs that adopt DC voltage droop control can be derived as

$$\Delta \mathbf{V}_{net} = \mathbf{C}_d (s\mathbf{E} - \mathbf{A}_d)^{-1} \mathbf{B}_d \Delta \mathbf{I}_{net} \quad (27)$$

where  $\Delta \mathbf{I}_{net} = [\Delta \bar{I}_{net1} \dots \Delta \bar{I}_{net(M-N)}]^T$ ,  $\Delta \mathbf{V}_{net} = [\Delta \bar{V}_1 \dots \Delta \bar{V}_{M-N}]^T$ , and  $\mathbf{A}_d = \text{diag}(\mathbf{a}_f^d)$ ,  $\mathbf{B}_d = \text{diag}(\mathbf{b}_f^d)$ ,  $\mathbf{C}_d = \text{diag}(\mathbf{c}_f^d)$ .

#### B. Linearized Model of the VSC-MTDC Power System

The transfer function of the MTDC network can be obtained using the analogy of (14) and (15) as

$$\Delta \mathbf{I}_{net} = -\mathbf{Y}_d(s) \Delta \mathbf{V}_{net} \quad (28)$$

By substituting (28) into (27), the characteristic equation of the VSC-MTDC power system with DC voltage droop control can be obtained as

$$\mathbf{C}_d (s\mathbf{E} - \mathbf{A}_d)^{-1} \mathbf{B}_d + \mathbf{Y}_d(s)^{-1} = \mathbf{0} \quad (29)$$

In (29), the  $M - N$  two-order parts of  $\mathbf{C}_d (s\mathbf{E} - \mathbf{A}_d)^{-1} \mathbf{B}_d$  are generated by the  $M - N$  DC voltage-controlled VSCs. Moreover, the dynamics of  $\mathbf{Y}_d(s)^{-1}$  are formed by the DC network and

capacitors of  $N$  active power-controlled VSCs. They are coupled through the MTDC network, and they collectively determine the stability of the DC voltage oscillation.

### C. Stability Analysis of DC Voltage Oscillation

In the VSC-MTDC power system with DC voltage droop control, to ensure the robustness of the analysis results, only the worst-case scenario is analyzed. Thus, the linearized model of VSC with the worst damping ratio ( $\mathbf{a}_w^d$ ,  $\mathbf{b}_w^d$ , and  $\mathbf{c}_w^d$ ) among the VSCs is used to represent all VSCs, thus yielding

$$\mathbf{a}_f^d = \mathbf{a}_w^d, \mathbf{b}_f^d = \mathbf{b}_w^d, \mathbf{c}_f^d = \mathbf{c}_w^d, f = 1, 2, \dots, M - N. \quad (30)$$

The open-loop DC voltage oscillation mode of the MTDC power system is denoted by  $\lambda_{d0} = -\varepsilon_{d0} + j\omega_{d0}$ , i.e., the solution of  $|s\mathbf{I} - \mathbf{a}_w^d| = 0$ . The damping ratio of  $\lambda_{d0}$  is  $d_{d0} = \varepsilon_{d0}(\sqrt{\varepsilon_{d0}^2 + \omega_{d0}^2})^{-1}$ . The DC voltage droop-controlled VSC is self-stable, and its impact is positive if  $\varepsilon_{d0} > 0$ , yielding

$$\bar{I}_w(1 + K_{aw}K_{pw}\bar{V}_w) - K_{rw}K_{pw}\bar{V}_w - C_w\bar{V}_wK_{iw}K_{aw}\bar{V}_w < 0. \quad (31)$$

The worst closed-loop DC voltage oscillation mode of the MTDC power system is denoted by  $\lambda_{dw} = -\varepsilon_{dw} + j\omega_{dw}$ . The damping ratio of  $\lambda_{dw}$  is  $d_{dw} = \varepsilon_{dw}(\sqrt{\varepsilon_{dw}^2 + \omega_{dw}^2})^{-1}$ . The impact of the MTDC network on the DC voltage oscillation can be evaluated using  $\Delta d_{dw}$ , where  $\Delta d_{dw} = d_{dw} - d_{d0}$ , which is positive if  $\Delta d_{dw} > 0$ .

At frequency  $\omega_{dw}$ ,  $\mathbf{Y}_d(s)$  becomes  $\mathbf{Y}_d(j\omega_{dw})$ . Further, the worst eigenvalue of  $\mathbf{Y}_d(j\omega_{dw})$  is  $\rho_w(j\omega_{dw}) = \rho_{gw}(\omega_{dw}) + j\rho_{hw}(\omega_{dw})$ . The stability of the DC voltage oscillation can be equivalently evaluated using the sub-characteristic equation below (Proven in Appendix B)

$$\begin{aligned} & \mathbf{c}_w^d(s\mathbf{E} - \mathbf{a}_w^d)^{-1}\mathbf{b}_w^d + \rho_w(j\omega_{dw})^{-1} \\ &= \frac{H_w^d(s)}{K_{w-1}^d s^2 + K_{w-2}^d s + K_{w-3}^d} + \frac{1}{\rho_{gw}(\omega_{dw}) + j\rho_{hw}(\omega_{dw})} \\ &\approx K_{w-1}^d s^2 + K_{w-2}^d s + K_{w-3}^d + T_1(\omega_{dw})s + T_2(\omega_{dw}) = 0 \end{aligned} \quad (32)$$

where

$$\begin{aligned} T_1(\omega_{dw}) &= (\bar{V}_w + \bar{V}_w\bar{V}_wK_{aw}K_{pw})\rho_{gw}(\omega_{dw}) \\ &+ \omega_{dw}^{-1}\bar{V}_w\bar{V}_wK_{aw}K_{iw}\rho_{hw}(\omega_{dw}) \\ T_2(\omega_{dw}) &= \bar{V}_w\bar{V}_wK_{aw}K_{iw}\rho_{gw}(\omega_{dw}) \\ &- (\bar{V}_w + \bar{V}_w\bar{V}_wK_{aw}K_{pw})\rho_{hw}(\omega_{dw})\omega_{dw} \end{aligned}$$

From (32),  $\Delta d_{dw}$  can be calculated as

$$\Delta d_{dw} = \frac{1}{2} \left( \frac{K_{w-2}^d + T_1(\omega_{dw})}{\sqrt{K_{w-1}^d(K_{w-3}^d + T_2(\omega_{dw}))}} - \frac{K_{w-2}^d}{\sqrt{K_{w-1}^d K_{w-3}^d}} \right). \quad (33)$$

From (33) and under the condition that  $\Delta d_{dw} > 0$ , the DC voltage oscillations are well damped and the MTDC power system is stable. If  $\Delta d_{dw} < 0$ , the damping ratio of  $\lambda_{dw}$  decreases. A three-terminal power system ( $M = 3$  in Fig. 1) is used as an example to explain the impact of the MTDC network on the DC voltage oscillation. Hereby, the 1<sup>st</sup> and 2<sup>nd</sup> VSC adopt DC voltage droop control and the 3<sup>rd</sup> VSC adopts active power control. At frequency  $\omega_{dw}$ , an assumed conductance matrix is

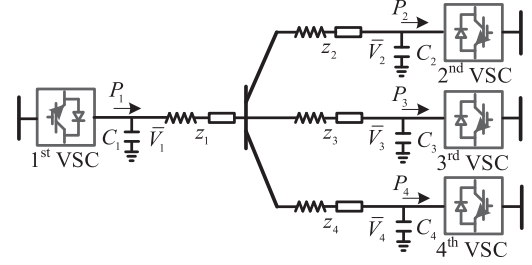


Fig. 4. A four-terminal VSC-MTDC power system adopting master-slave control.

defined in (34) for simple analysis:

$$\begin{bmatrix} \Delta \bar{I}_{net1} \\ \Delta \bar{I}_{net2} \\ \Delta \bar{I}_{net3} \end{bmatrix} = - \begin{bmatrix} y & -y \\ & y & -y \\ -y & -y & 2y \end{bmatrix} \begin{bmatrix} \Delta \bar{V}_1 \\ \Delta \bar{V}_2 \\ \Delta \bar{V}_3 \end{bmatrix}, \quad (34)$$

where  $\Delta \bar{V}_3 = R_{e3}(j\omega_{dw})\Delta \bar{I}_{net3}$ .

According to (28) and (34), the eigenvalues of  $\mathbf{Y}_d(j\omega_{dw})$  are calculated as

$$\rho_1(j\omega_{dw}) = y, \rho_w(j\omega_{dw}) = \frac{y}{2R_{e3}(j\omega_{dw})y + 1} \quad (35)$$

From (35), it can be seen that  $\rho_w(j\omega_{dw})$  is not related to the VSC control parameters. However, it is closely related to the power flow of the 3<sup>rd</sup> VSC. When the 3<sup>rd</sup> VSC changes its function from power dispersion ( $I_{dc30} < 0$ ) to power absorption ( $I_{dc30} > 0$ ), the equivalent impedance of the 3<sup>rd</sup> VSC, i.e.,  $R_{e3}(j\omega_{dw})$ , becomes negative, which may result in  $\rho_w(j\omega_{dw}) < 0$ . Subsequently, the stability of the DC voltage oscillation decreases if  $\Delta d_{dw} < 0$ . To maintain the stability of the DC voltage oscillation, the capacity of the constant power loads should be restricted. The limitation of  $\rho_{gw}(\omega_{dw})$  can be obtained as  $\rho_{lim}$  using (36).

$$\rho_{lim}(\omega_{dw}) = -\frac{K_{w-2}^d C_w}{K_{w-1}^d} - \frac{\bar{V}_w\bar{V}_wK_{aw}K_{iw}\rho_{hw}(\omega_{dw})}{\omega_{dw}(\bar{V}_w + \bar{V}_w\bar{V}_wK_{pw}K_{aw})} \quad (36)$$

DC voltage oscillations may occur if the following limitation is exceeded:

$$\rho_{gw}(\omega_{dw}) > \rho_{lim}(\omega_{dw}) \quad (37)$$

Hence, under the condition that the VSCs are self stable, the DC voltage oscillation is stable as long as the constant power loads are eliminated, or they are within defined limits of (37). To quickly determine the stability risk of the VSC-MTDC power system, the frequency range  $[\omega_{min}, \omega_{max}]$ , where  $\omega_{max} \geq \omega_{dw} \geq \omega_{min}$  is selected. By sweeping frequency in the frequency range, the stability of the DC voltage oscillation can be quickly determined with (37).

### IV. CASE STUDY 1—MASTER-SLAVE-CONTROLLED VSC-MTDC POWER SYSTEM

The configuration of an exemplified MTDC power system adopting master-slave control is shown in Fig. 4. The configuration is radial and includes four VSC stations. The 1<sup>st</sup> VSC

TABLE I  
CALCULATED RESULTS OF THE VSC-MTDC SYSTEM (MASTER-SLAVE CONTROL)

VSC	Open-loop DC oscillation mode	$G_{lim} = -0.08$ $G_{min} = 0.395$ $G_m(j\omega_m) = 0.51$	Closed-loop DC oscillation mode
1	$-2.28 + j82.82$		$-4.16 + j41.23$
2-4			

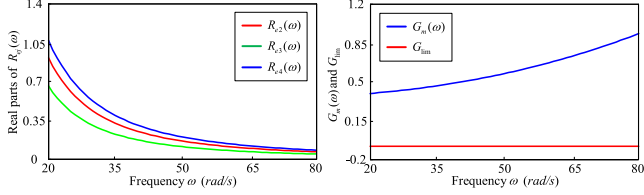


Fig. 5. Frequency sweeping results of the VSC-MTDC system (master-slave control).

adopts DC voltage control. The remaining VSCs adopt active power control. Details of the parameters and loading conditions are provided in Table V in Appendix C [21]–[23].

#### A. Validation of the Analysis Results

Initially, the open-loop DC voltage oscillation mode of each VSC is calculated based on the linearized model described in (7) to ensure individual stability of each VSC. From the 2<sup>nd</sup> column of Table I, it can be observed that the 1<sup>st</sup> VSC shows a stable open-loop DC voltage oscillation mode, while the other VSCs adopting active power control show no DC voltage oscillation mode. The DC voltage oscillation is caused by the DC voltage-controlled VSC when master–slave control is applied to the VSC-MTDC power system.

The equivalent impedances of the active power-controlled VSCs in the frequency range from  $\omega_{min} = 20$  rad/s to  $\omega_{max} = 80$  rad/s, are shown in Fig. 5. Because the VSCs inject power into the MTDC power system, the equivalent impedance of each VSC is positive. Thus, the MTDC power system will not be unstable. This conclusion is further verified as follows.

The equivalent conductance of the MTDC network including the VSCs adopting active power control is shown in Fig. 5 by sweeping the frequencies in the frequency range.  $G_{min}$  is determined to be 0.395 at 20 rad/s. According to (22),  $G_{lim}$  is calculated to be  $-0.08$ . Obviously,  $G_{min}$  is larger than the limitation of  $G_{lim}$ . Therefore, the DC voltage oscillation is considered to be stable in this frequency range.

Based on (16), the strict closed-loop DC voltage oscillation mode is calculated to be  $-4.16 + j41.23$  and its damping ratio is better than that of the open-loop DC voltage oscillation mode. The DC voltage oscillation is stable in the MTDC power system with no constant power loads. At frequency  $\omega_m = 41.23$  rad/s, the conductance of the MTDC network  $G_m(\omega_m)$  is 0.51 and  $\frac{K_2^m}{V_1}(\sqrt{1 - \frac{\omega_m \bar{V}_1 H_m(\omega_m)}{K_3^m}} - 1)$  is  $-0.02$ . Thus, the condition listed in (20) is satisfied, indicating that the impact of the MTDC network is also positive.

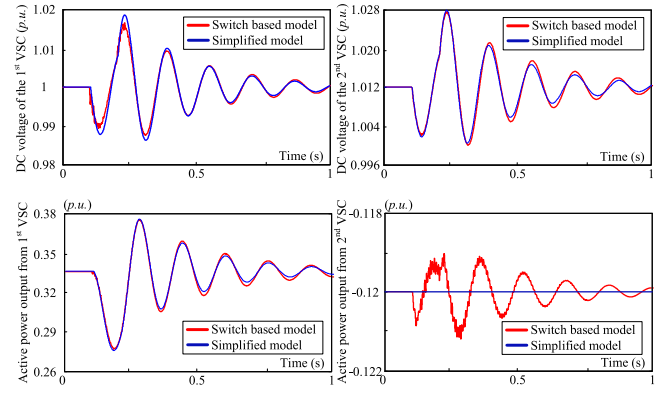


Fig. 6. Nonlinear simulation results (master–slave control).

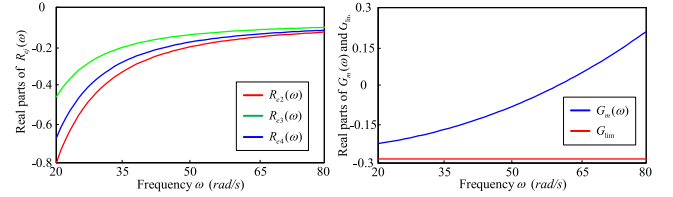


Fig. 7. Frequency-sweeping results of the VSC-MTDC system (power flow is reversed).

For further confirmation, the standard SIMULINK model is established, where the 1980-Hz 3-level 3-phase VSC in the SimPowerSystems-Toolbox is adopted [23]. The VSC control system uses two control loops: an external control loop which regulates DC voltage and internal control loop which regulates grid currents. Voltage outputs of the current controller are converted to three modulating signals used by the PWM generator. A comparison between the nonlinear simulation results based on the SIMULINK model and those based on the reduced model of (16) are shown in Fig. 6. At 0.1 s, the active power injected into the MTDC power system suddenly drops by 0.06 p.u. and recovers at 0.2 s. This finding confirms that the variation in active power output from the 2<sup>nd</sup> VSC is weak. Thus, the active power-controlled VSC can be considered as a constant power source. Moreover, overlooking the fast dynamics of the MTDC system in the bandwidth range of the DC voltage oscillation has little effect on the results. Thus, the validity of the analyzed conclusions is verified.

#### B. Instability Caused by Reversing Power Flow

In this subsection, the power flow reversal is considered and the parameters of VSCs are appropriately designed to stabilize the open-loop DC voltage oscillation mode. The DC powers injected by the 2<sup>nd</sup>, 3<sup>rd</sup>, and 4<sup>th</sup> VSCs are 0.1, 0.05, and 0.08 p.u., respectively. The frequency-sweeping results are shown in Fig. 7, and the calculated results are listed in Table II. Considering that the active power-controlled VSCs absorb power from the MTDC power system as constant power loads, the equivalent impedance of each VSC is negative. This may reduce the stability

TABLE II  
CALCULATED RESULTS OF THE VSC-MTDC SYSTEM (POWER FLOW IS REVERSED)

VSC	Open-loop DC oscillation mode	$G_{lim} = -0.29$ $G_{min} = -0.22$ $G_m(j\omega_m) = -0.12$	Closed-loop DC oscillation mode
1	$-8.31 + j82.43$		$-1.19 + j40.98$
2-4			

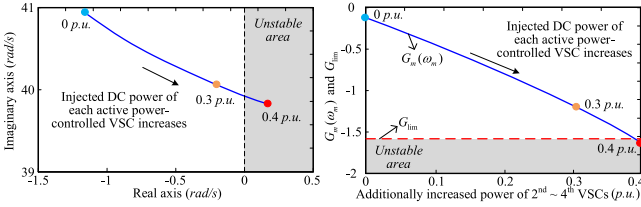


Fig. 8. Trajectories of the DC oscillation modes,  $G_m(\omega_m)$  and  $G_{lim}$ .

of the MTDC system and, in the worst case, cause DC voltage oscillations.

From Fig. 7, the equivalent conductance of the MTDC network in the frequency range of  $20 \sim 80$  rad/s is negative. At frequency  $\omega_m = 40.98$  rad/s,  $G_m(\omega_m) = -0.15$  and  $\frac{K_2^m}{V_1}(\sqrt{1 - \frac{\omega_m V_1 H_m(\omega_m)}{K_3^m}} - 1) = -0.14$ , so  $G_m(\omega_m) < -0.14$ . This indicates that the damping ratio of the closed-loop DC voltage oscillation mode decreases and is negatively affected by the constant power loads. However, the DC voltage oscillation cannot be unstable because  $G_{min} > G_{lim}$ . A complex calculation of the closed-loop DC voltage oscillation mode is shown in the 4<sup>th</sup> column of Table II. The result confirms the conclusion that the damping ratio of the closed-loop DC voltage oscillation mode is worse than that of the open-loop DC voltage oscillation mode. The instability of the DC voltage oscillation can be eliminated by limiting the maximum transmitted power when a negative conductance is detected. This can be verified as follows.

The DC power injected by the 2<sup>nd</sup>, 3<sup>rd</sup>, and 4<sup>th</sup> VSCs is additionally increased from 0 to 0.4 p.u. The trajectories of the DC voltage oscillation modes,  $G_m(\omega_m)$  and  $G_{lim}$ , are shown in Fig. 8. From this figure, it can be observed that  $G_m(\omega_m)$  is close to  $G_{lim}$  and the damping ratio of the DC voltage oscillation mode decreases with an increase in the transmitted power. When the additionally transmitted power approaches 0.4 p.u.,  $G_m(\omega_m)$  exceeds the limitation; thus, the DC voltage oscillation mode loses its stability.

For additionally increased power of 0.3 p.u., a comparison of the nonlinear simulation results is shown in Fig. 9. At 0.1 s, the active power injected into the MTDC system suddenly drops by 0.07 p.u. and recovers at 0.2 s. DC voltage oscillations occur, confirming the validity of the analysis results given in Table II and shown in Fig. 8.

## V. CASE STUDY 2—DC VOLTAGE DROOP-CONTROLLED VSC-MTDC POWER SYSTEM

The configuration of a complex MTDC network comprising a four-terminal VSC-MTDC system is shown in Fig. 10. The 1<sup>st</sup> and 2<sup>nd</sup> VSCs adopt DC voltage droop control, and the remaining

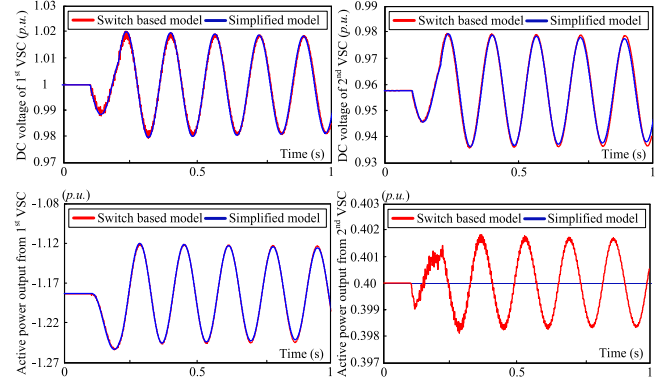


Fig. 9. Nonlinear simulation results (master-slave control).

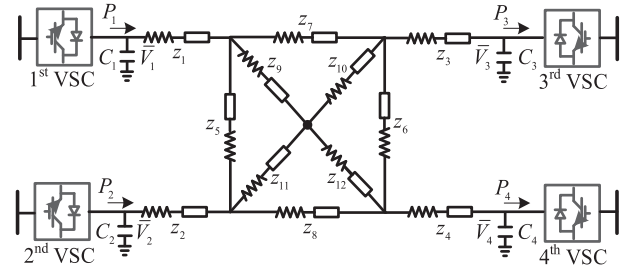


Fig. 10. A four-terminal VSC-MTDC power system adopting DC voltage droop control.

TABLE III  
CALCULATED RESULTS OF THE VSC-MTDC SYSTEM (DC VOLTAGE DROOP CONTROL)

VSC	Open-loop DC oscillation mode	$\rho_{gv}(j\omega_{dv}) = 0.18$ $\rho_{lm}(j\omega_{dv}) = -0.19$	Worst closed-loop DC oscillation mode
1	$-2.57 + j81.12$		$-5.27 + j57.26$
2	$-2.42 + j81.10$		
3-4			

VSCs adopt active power control. Details of the parameters and loading conditions are given in Table VI in Appendix C.

The analysis and evaluation procedure for the DC voltage oscillation stability are similar to those of the master-slave-controlled MTDC system. A major enhancement in the investigation of the stability of this multi-input multi-output system is the use of the eigenvalues of the conductance matrix. The details are given below.

### A. Validation of the Analyzed Conclusions

The open-loop DC voltage oscillation modes of the VSCs are given in the 2<sup>nd</sup> column of Table III. The 1<sup>st</sup> and 2<sup>nd</sup> VSCs show stable open-loop DC voltage oscillation modes. Similar to the master-slave-controlled DC system, the VSCs that adopt active power control show no DC voltage oscillation mode.

In the frequency range from  $\omega_{min} = 20$  rad/s to  $\omega_{max} = 80$  rad/s, the active power-controlled VSC is equivalent to a positive constant impedance (Fig. 11) because these VSCs inject power into the MTDC system. Therefore, in this case, the MTDC



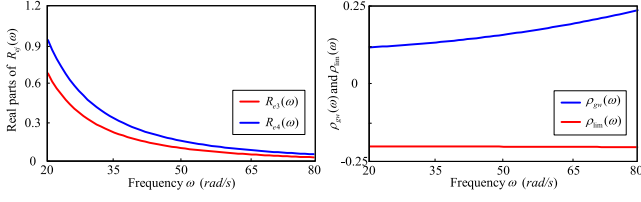


Fig. 11. Frequency-sweeping results of the VSC-MTDC system (DC voltage droop control).

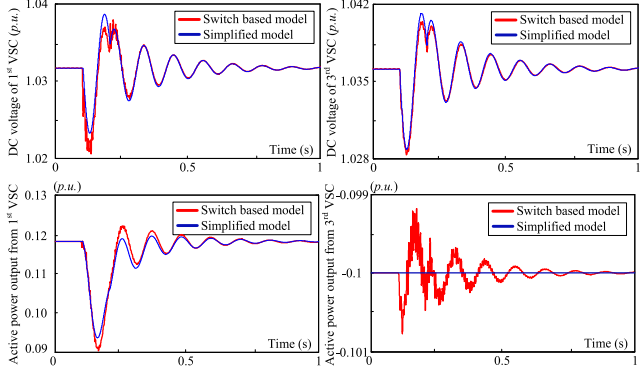


Fig. 12. Nonlinear simulation results (DC voltage droop control).

system will not be unstable. This finding is further confirmed as follows.

Based on (29), the worst closed-loop DC voltage oscillation mode is calculated to be  $-5.27 + j57.26$ , and its damping ratio is better than that of the open-loop DC voltage oscillation mode. The DC voltage oscillation is stable in the MTDC power system with no constant power loads. At frequency  $\omega_{dw} = 57.26$  rad/s, the conductance of the MTDC network is positive, i.e.,  $\rho_{gw}(\omega_{dw}) = 0.18$ , which is larger than the limitation, i.e.,  $\rho_{lim}(\omega_{dw}) = -0.19$ . This result demonstrates that if the eigenvalues of the conductance matrix are positive, the DC voltage oscillation is stable.

A comparison of the nonlinear simulation results is shown in Fig. 12. At 0.1 s, the active power injected from the 1<sup>st</sup> VSC into the MTDC system suddenly drops by 0.028 p.u. and recovers at 0.2 s. This result confirms that overlooking the fast dynamics of the MTDC system in the bandwidth range of DC voltage oscillation has little effect on the results.

### B. Instability Caused by Reverse Power Flow

The results for the case where the power flow is reversed and the DC powers injected by the 3<sup>rd</sup> and 4<sup>th</sup> VSCs are 0.1 and 0.2 p.u., respectively, are given in Table IV. The open-loop DC voltage oscillation modes of the two VSCs adopting DC voltage droop control are appropriately designed. However, the equivalent impedances of the 3<sup>rd</sup> and 4<sup>th</sup> VSCs are negative because the VSCs absorb power from the DC system, thus acting as constant power loads. This may reduce the stability of the DC voltage oscillation.

The frequency-sweeping results are shown in Fig. 13, and the calculated results at frequency  $\omega_{dw} = 57.48$  rad/s are given

TABLE IV  
CALCULATED RESULTS OF THE VSC-MTDC SYSTEM (POWER FLOW IS REVERSED)

VSC	Open-loop DC oscillation mode	$\rho_{gw}(j\omega_{dw}) = -0.102$	Worst closed-loop DC oscillation mode
1	$-7.50 + j82.09$	$\rho_{lim}(j\omega_{dw}) = -0.37$	$-3.83 + j57.48$
2	$-7.76 + j82.10$		
3 ~ 4			

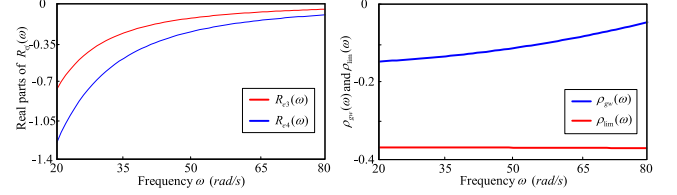
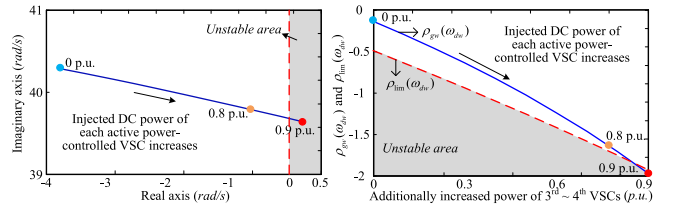


Fig. 13. Frequency-sweeping results of the VSC-MTDC system (power flow is reversed).


 Fig. 14. Trajectories of the DC oscillation modes,  $\rho_{gw}(\omega_{dw})$  and  $\rho_{lim}(\omega_{dw})$ .

in Table IV.  $\rho_{gw}(\omega_{dw})$  is negative, indicating that the constant power loads may have a negative impact on DC voltage oscillation stability. Because  $\rho_{gw}(\omega_{dw})$  is larger than  $\rho_{lim}(\omega_{dw})$ , the DC voltage oscillation mode is stable.

The DC power injected by the 3<sup>rd</sup> and 4<sup>th</sup> VSCs is additionally increased from 0 to 0.9 p.u. The trajectories of the worst DC voltage oscillation modes,  $\rho_{gw}(\omega_{dw})$  and  $\rho_{lim}(\omega_{dw})$ , are shown in Fig. 14. From this figure, it can be observed that  $\rho_{gw}(\omega_{dw})$  is close to  $\rho_{lim}(\omega_{dw})$ ; thus, the damping ratio of the DC voltage oscillation mode decreases with an increase in the transmitted power. When the additionally increased power approaches 0.9 p.u., the limitation of  $\rho_{gw}(\omega_{dw})$  is exceeded and the DC voltage oscillation becomes unstable.

A comparison of the nonlinear simulation results based on the MATLAB SIMULINK model and reduced model when the additionally increased power is 0.8 p.u. is shown in Fig. 15. At 0.1 s, the active power injected from the 1<sup>st</sup> VSC into the DC system suddenly drops by 0.04 p.u. and recovers at 0.2 s. DC voltage oscillation occurs, thus confirming the validity of the analysis results given in Table IV and shown in Fig. 14.

## VI. CONCLUSION

In this study, the DC voltage oscillation mechanism was theoretically investigated and verified using the standard MATLAB SIMULINK model. It was confirmed for the first time that the inner dynamics of the MTDC system as well as the

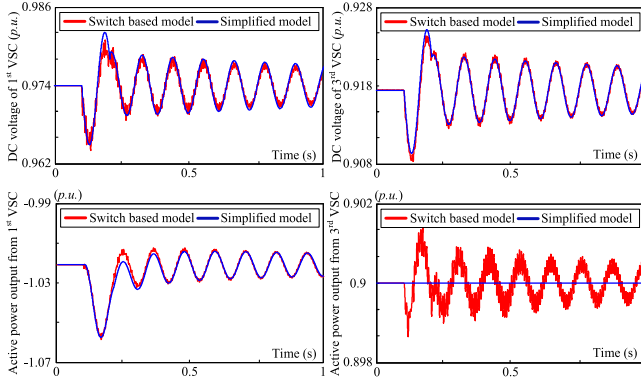


Fig. 15. Nonlinear simulation results (DC voltage droop control).

steady-state power flow affects the stability of the DC voltage oscillation. These findings are beneficial for engineers because new instability risks within the MTDC system are revealed in addition to traditional instability risks caused by the dynamics of the AC system. The conclusions are summarized as follows:

- 1) A VSC that adopts DC voltage control or DC voltage droop control is the source of DC voltage oscillation, whereas a VSC that adopts active power control can be considered as a constant power source.
- 2) The DC voltage oscillation is affected by the dynamics of VSCs and the interactions caused by the MTDC network. Even if the parameters of VSCs are appropriately designed to ensure the self-stability of the VSC, DC voltage oscillation instability can still occur because the MTDC network may have a negative impact on the DC voltage oscillation mode.
- 3) The negative impact of the MTDC network is induced by constant power loads or when the power flow is reversed. The stability of the DC voltage oscillation reduces either in the master-slave-controlled or the DC voltage droop-controlled MTDC power system when the eigenvalues of the conductance matrix decrease. Limiting the maximum transmitted power can improve the stability of the DC voltage oscillation.

#### APPENDIX A

Detail derivation results of (7)

$$\begin{aligned} \mathbf{x}_1^m &= [\Delta \bar{V}_1 \ \Delta \tilde{I}_{d1}]^T, \\ \mathbf{b}_1^m &= [C_1^{-1} \ K_{p1} C_1^{-1}]^T, \ \mathbf{a}_1^m = \begin{bmatrix} \frac{\bar{I}_1}{C_1 V_1} & -\frac{\tilde{V}_1}{C_1 V_1} \\ \frac{\bar{I}_1 K_{p1}}{C_1 V_1} + K_{i1} & -\frac{\tilde{V}_1 K_{p1}}{C_1 V_1} \end{bmatrix} \\ \mathbf{c}_1^m &= [1 \ 0], \end{aligned} \quad (\text{A1})$$

Detail derivation results of (11)

$$\begin{aligned} \mathbf{x}_j^m &= [\Delta \bar{V}_j \ \Delta \tilde{I}_{dj}]^T, \\ \mathbf{b}_j^m &= [C_j^{-1} \ 0]^T, \ \mathbf{a}_j^m = \begin{bmatrix} \frac{\bar{I}_{netj}}{C_j \bar{V}_j} & -\frac{\tilde{V}_j}{C_j \bar{V}_j} \\ 0 & -\frac{K_{ij} \bar{V}_j}{1 + K_{pj} \bar{V}_j} \end{bmatrix} \\ \mathbf{c}_j^m &= [1 \ 0], \end{aligned} \quad (\text{A2})$$

Detail derivation results of (25)

$$\mathbf{x}_f^d = [\Delta \bar{V}_f \ \Delta \tilde{I}_{df}]^T, \ \mathbf{c}_f^d = [1 \ 0],$$

$$\begin{aligned} \mathbf{b}_f^d &= \left[ \frac{1}{C_f} \ \frac{K_{rf} K_{pf}}{C_f + C_f K_{af} K_{pf} \bar{V}_f} \right]^T \\ \mathbf{a}_f^d &= \begin{bmatrix} a_{11} & a_{12} \\ a_{21} & a_{22} \end{bmatrix}, \ a_{11} = \frac{\bar{I}_{netf}}{C_f \bar{V}_f}, \ a_{12} = -\frac{1}{C_f \bar{V}_f} \tilde{V}_f \\ a_{21} &= \frac{K_{rf} K_{pf} \bar{I}_{netf}}{C_f \bar{V}_f (1 + K_{af} K_{pf} \bar{V}_f)} + \frac{K_{if} K_{rf}}{1 + K_{af} K_{pf} \bar{V}_f} \\ a_{22} &= -\frac{K_{rf} K_{pf} \tilde{V}_f}{C_f \bar{V}_f (1 + K_{af} K_{pf} \bar{V}_f)} - \frac{K_{if} K_{af} \tilde{V}_f}{1 + K_{af} K_{pf} \bar{V}_f} \end{aligned} \quad (\text{A3})$$

#### APPENDIX B

There exists a matrix  $\mathbf{P}_c$  such that  $\mathbf{P}_c \mathbf{Y}_d(j\omega_{dw}) \mathbf{P}_c^{-1} = \text{diag}(\rho_f(j\omega_{dw}))$ ,  $\mathbf{P}_c \mathbf{P}_c^{-1} = \mathbf{E}$ , where  $\mathbf{P}_c \in R^{(M-N) \times (M-N)}$ ,  $\text{diag}(\rho_f(j\omega_{dw}))$  refers to a diagonal matrix and  $\rho_w(j\omega_{dw})$  is the worst eigenvalue among  $\rho_f(j\omega_{dw})$ .

From (28) and (29) [20],

$$\begin{aligned} &\mathbf{C}_d(s\mathbf{E} - \mathbf{A}_d)^{-1} \mathbf{B}_d + \mathbf{Y}_d(j\omega_{dw})^{-1} \\ &= \text{diag}[\mathbf{c}_w^d] \text{diag}[(s\mathbf{E} - \mathbf{a}_w^d)^{-1}] \text{diag}[\mathbf{b}_w^d] + \mathbf{Y}_d(j\omega_{dw})^{-1} = \mathbf{0} \end{aligned} \quad (\text{B1})$$

By multiplying  $\mathbf{P}_c \otimes \mathbf{E}$  and  $\mathbf{P}_c^{-1} \otimes \mathbf{E}$  with (B1), it can be transformed to be

$$\begin{aligned} &[\mathbf{P}_c \otimes \mathbf{E}] \text{diag}[\mathbf{c}_w^d] \text{diag}[(s\mathbf{E} - \mathbf{a}_w^d)^{-1}] \text{diag}[\mathbf{b}_w^d] [\mathbf{P}_c^{-1} \otimes \mathbf{E}] \\ &+ [\mathbf{P}_c \otimes \mathbf{E}] \mathbf{Y}_d(j\omega_{dw})^{-1} [\mathbf{P}_c^{-1} \otimes \mathbf{E}] \\ &= \text{diag}[\mathbf{c}_w^d] \text{diag}[(s\mathbf{E} - \mathbf{a}_w^d)^{-1}] \text{diag}[\mathbf{b}_w^d] \\ &+ [(\mathbf{P}_c \otimes \mathbf{E}) \mathbf{Y}_d(j\omega_{dw}) (\mathbf{P}_c^{-1} \otimes \mathbf{E})]^{-1} \\ &= \text{diag}[\mathbf{c}_w^d (s\mathbf{E} - \mathbf{a}_w^d)^{-1} \mathbf{b}_w^d + \rho_f(j\omega_{dw})^{-1}] \end{aligned} \quad (\text{B2})$$

Hence,  $\mathbf{C}_d(s\mathbf{E} - \mathbf{A}_d)^{-1} \mathbf{B}_d + \mathbf{Y}_d(j\omega_{dw})^{-1} = \mathbf{0}$  is similar to  $\text{diag}[\mathbf{c}_w^d (s\mathbf{E} - \mathbf{a}_w^d)^{-1} \mathbf{b}_w^d + \rho_f(j\omega_{dw})^{-1}] = \mathbf{0}$ . The sub-characteristic equation with the worst DC voltage oscillation mode is  $\mathbf{c}_w^d (s\mathbf{E} - \mathbf{a}_w^d)^{-1} \mathbf{b}_w^d + \rho_w(j\omega_{dw})^{-1} = 0$ .

#### APPENDIX C

TABLE V  
PARAMETERS OF THE VSC-MTDC SYSTEM IN FIG. 4

Parameters	Value
Direct voltages of	$V_{dc1} = 1.0$ p.u., $V_{dc2} = 1.012$ p.u.,
VSC-1 ~ VSC-4.	$V_{dc3} = 1.0045$ p.u., $V_{dc4} = 1.0147$ p.u.,
Input power of	$P_{s1} = 0.337$ p.u., $P_{s2} = -0.12$ p.u.,
VSC-1 ~ VSC-4.	$P_{s3} = -0.08$ p.u., $P_{s4} = -0.15$ p.u.,
Capacitances of	$C_1 = 6.59$ p.u., $C_2 = 6.59$ p.u.,
VSC-1 ~ VSC-4.	$C_3 = 6.59$ p.u., $C_4 = 6.59$ p.u.,
Control parameters	$K_{p1} = 0.35, K_{i1} = 120, K_{p2} = 0.1, K_{i2} = 20,$
of VSC-1 ~ VSC-4.	$K_{p3} = 0.1, K_{i3} = 20, K_{p4} = 0.1, K_{i4} = 20.$
Impedance of the	$z_1 = 0.0024 + j0.0045$ p.u., $z_2 = 0.095 + j0.178$ p.u.,
transmission lines.	$z_3 = 0.0475 + j0.089$ p.u., $z_4 = 0.095 + j0.178$ p.u.,
Fundamental	1.0 p.u.
frequency.	

TABLE VI  
PARAMETERS OF THE VSC-MTDC SYSTEM IN FIG. 10

Parameters	Value
Direct voltages of VSC-1 ~ VSC-4.	$V_{dc1} = 1.0309$ p.u., $V_{dc2} = 1.0311$ p.u., $V_{dc3} = 1.0369$ p.u., $V_{dc4} = 1.0382$ p.u..
Input power of VSC-1 ~ VSC-4.	$P_{s1} = 0.1185$ p.u., $P_{s2} = 0.1215$ p.u., $P_{s3} = -0.10$ p.u., $P_{s4} = -0.15$ p.u..
Capacitances of VSC-1 ~ VSC-4.	$C_1 = 6.59$ p.u., $C_2 = 6.59$ p.u., $C_3 = 6.59$ p.u., $C_4 = 6.59$ p.u..
Control parameters of VSC-1 ~ VSC-4.	$K_{p1}=0.1, K_{i1}=120, K_{r1}=1, K_{a1}=0.05$ , $K_{p2}=0.1, K_{i2}=120, K_{r2}=1, K_{a2}=0.05$ , $K_{p3}=0.1, K_{i3}=20$ , $K_{p4}=0.1, K_{i4}=20$ .
Impedance of the transmission lines.	$z_1 \sim z_4 = 0.0119 + j0.0223$ p.u., $z_5 = z_6 = 0.0713 + j0.1335$ p.u., $z_7 \sim z_{12} = 0.0475 + j0.089$ p.u..
Fundamental frequency.	1.0 p.u.

## REFERENCES

- [1] M. Ashourianjozdani, L. A. C. Lopes, and P. Pillay, "Power electronic converter based PMSG emulator: A testbed for renewable energy experiments," *IEEE Trans. Ind. Appl.*, vol. 54, no. 4, pp. 3626–3636, Aug. 2018.
- [2] W. Du, Q. Fu, and H. Wang, "Small-Signal stability of an AC/MTDC power system as affected by open-loop modal coupling between the VSCs," *IEEE Trans. Power Syst.*, vol. 33, no. 3, pp. 3143–3152, May. 2018.
- [3] A. Bayo-Salas, J. Beerten, J. Rimez, and D. Van Hertem, "Analysis of control interactions in multi-infeed VSC HVDC connections," *IET Gener., Transm. Distrib.*, vol. 10, no. 6, pp. 1336–1344, May 2016.
- [4] W. Du, Y. Wang, H. F. Wang, B. Ren, and X. Xiao, "Small-disturbance stability limit of a Grid-connected wind farm with PMSGs in the timescale of DC voltage dynamics" *IEEE Trans. Power Syst.*, early access, 2020.
- [5] N. Chaudhuri, R. Majumder, B. Chaudhuri, and J. Pan, "Stability analysis of VSC MTDC grids connected to multimachine AC systems," *IEEE Trans. Power Del.*, vol. 26, no. 4, pp. 2774–2784, Oct. 2011.
- [6] W. Du, Q. Fu, and H. Wang, "Subsynchronous oscillations caused by open-loop modal coupling between VSC-based HVDC line and power system," *IEEE Trans. Power Syst.*, vol. 33, no. 4, pp. 3664–3677, Jul. 2018.
- [7] W. Wang, M. Barnes, O. Marjanovic, and O. Cwikowski, "Impact of DC breaker systems on multiterminal VSC-HVDC stability," *IEEE Trans. Power Del.*, vol. 31, no. 2, pp. 769–779, Apr. 2016.
- [8] M. K. Bucher, R. Wiget, and G. Andersson, "Multiterminal HVDC networks—What is the preferred topology?," *IEEE Trans. Power Del.*, vol. 29, no. 1, pp. 406–413, Feb. 2014.
- [9] W. Du, Q. Fu, and H. Wang, "Open-loop modal coupling analysis for a multi-input multi-output interconnected MTDC/AC power system," *IEEE Trans. Power Syst.*, vol. 34, no. 1, pp. 246–256, Jan. 2019.
- [10] Z. Wang, K. Li and J. Ren *et al.*, "A coordination control strategy of voltage-source-converter-based MTDC for offshore wind farms," *IEEE Trans. Ind. Appl.*, vol. 51, no. 4, pp. 2743–2752, Aug. 2015.
- [11] G. O. Kalcon, G. P. Adam, O. Anaya-Lara, S. Lo, and K. Uhlen, "Small-Signal stability analysis of multi-terminal VSC-based DC transmission systems," *IEEE Trans. Power Syst.*, vol. 27, no. 4, pp. 1818–1830, Nov. 2012.
- [12] N. R. Chaudhuri and B. Chaudhuri, "Adaptive droop control for effective power sharing in multi-terminal DC (MTDC) grids," *IEEE Trans. Power Syst.*, vol. 28, no. 1, pp. 21–29, Feb. 2013.
- [13] J. Beerten, S. D'Arco, and J. A. Suul, "Identification and small-signal analysis of interaction modes in VSC MTDC systems," *IEEE Trans. Power Del.*, vol. 31, no. 2, pp. 888–897, Apr. 2016.
- [14] D. Lu, X. Wang, and F. Blaabjerg, "Impedance-based analysis of DC-Link voltage dynamics in voltage-source converters," *IEEE Trans. Power Electron.*, vol. 34, no. 4, pp. 3973–3985, Apr. 2019.
- [15] H. Yuan, X. Yuan, and J. Hu, "Modeling of grid-connected VSCs for power system small-signal stability analysis in DC-Link voltage control timescale," *IEEE Trans. Power Syst.*, vol. 32, no. 5, pp. 3981–3991, Sep. 2017.
- [16] Y. Huang, X. Zhai, J. Hu, D. Liu, and C. Lin, "Modeling and stability analysis of VSC internal voltage in DC-Link voltage control timescale," *IEEE J. Em. Sel. Top. P.*, vol. 6, no. 1, pp. 16–28, Mar. 2018.
- [17] G. Pinares, and M. Bongiorno, "Modeling and analysis of VSC-based HVDC systems for DC network stability studies," *IEEE Trans. Power Del.*, vol. 31, no. 2, pp. 848–856, Apr. 2016.
- [18] H. F. Wang, and W. Du, *Analysis and Damping Control of Power System Low-Frequency Oscillations*, Berlin, Germany: Springer, 2016.
- [19] W. Du, Q. Fu, and H. Wang, "Damping torque analysis of DC voltage stability of an MTDC network for the wind power delivery," *IEEE Trans. Power Del.*, vol. 35, no. 1, pp. 324–338, Feb. 2020.
- [20] W. Du, Y. Wang, H. F. Wang, J. Yu, and X. Xiao, "Collective impact of multiple doubly fed induction generators with similar dynamics on the oscillation stability of a grid-connected wind farm," *IEEE Trans. Power Del.*, early access, 2020.
- [21] M. Amin, M. Zadeh, and J. A. Suul, "Stability analysis of interconnected AC power systems with multi-terminal DC grids based on the cigré DC grid test system," in *Proc. 3rd Renewable Power Gener. Conf. (RPG 2014)*, Naples, 2014, pp. 1–6.
- [22] K. Rouzbehi, A. Miranian, J. I. Candela, A. Luna, and P. Rodriguez, "A generalized voltage droop strategy for control of multiterminal DC grids," *IEEE Trans. Ind. Appl.*, vol. 51, no. 1, pp. 607–618, Jan./Feb. 2015.
- [23] Math Works, Inc., "Documentation center, simpowersystems," 2014.